Available online at www.sciencedirect.com
SCIENCE DIRECT®
Journal of Solid State Chemistry 177 (2004) 1244–1251
JOURNAL OF SOLID STATE CHEMISTRY
http://elsevier.com/locate/jssc

Formation of transition metal boride and carbide perovskites related to superconducting $MgCNi_3$

R.E. Schaak,[a,*] M. Avdeev,[b] W.-L. Lee,[c] G. Lawes,[d] H.W. Zandbergen,[a,e] J.D. Jorgensen,[b] N.P. Ong,[c] A.P. Ramirez,[d] and R.J. Cava[a]

[a] *Department of Chemistry and Princeton Materials Institute, Princeton University, Princeton, NJ 08544, USA*
[b] *Argonne National Laboratory, Materials Science Division, Argonne, IL 60439, USA*
[c] *Department of Physics, Princeton University, Princeton, NJ 08544, USA*
[d] *Condensed Matter and Thermal Physics Group, Los Alamos National Laboratory, Los Alamos, NM 87545, USA*
[e] *Laboratory for Materials Science, National Centre for HREM, Delft University of Technology, Rotterdamseweg 137, 2628 AL Delft, The Netherlands*

Received 14 August 2003; received in revised form 22 October 2003; accepted 26 October 2003

Abstract

A general study of the formation of intermetallic perovskite borides and carbides in the ternary systems AXM_3 (A = Mg, Ca, Sc, Y, Lu, Zr, Nb; X = B, C; M = Ni, Ru, Rh, Pd, Pt) is reported. MgB_xPd_3, MgB_xPt_3, CaB_xPd_3, MgC_xRh_3, LuC_xRh_3, and ZrC_xRh_3 represent new intermetallic perovskites that form at a composition that is nominally stoichiometric ($x = 1$). ScB_xPd_3, YB_xPd_3, and NbB_xRh_3 are new single-phase perovskites that form only at a substoichiometric ($x < 1$) nominal composition. The variable boron content of AB_xPd_3 (A = Mg, Ca, Sc, Y) was studied using lattice parameter data from X-ray diffraction measurements. For A = Ca and Mg, the unit cell volume increases with increasing boron content for $0.25 \leqslant x \leqslant 1.0$, while boron uptake is limited to $0 \leqslant x \leqslant 0.5$ for A = Sc and Y. Neutron diffraction studies indicate that CaB_xPd_3 is not actually stoichiometric at a nominal composition of $x = 1$. Rather, saturation of the boron content occurs at $CaB_{0.76}Pd_3$. Evidence for superconductivity was found in samples of CaB_xPd_3 ($x \geqslant 1$) and NbB_xRh_3, but bulk analysis suggests that superconductivity may be attributed to minority phases.

Keywords: Intermetallic superconductor; Intermetallic perovskite; Neutron diffraction; Crystal structure; Substoichiometric compounds; Superconductivity

1. Introduction

The recent discovery of superconductivity in the intermetallic perovskite $MgCNi_3$ provides a unique structural link between high-T_c cuprate superconductors and intermetallic superconductors [1]. Perovskite intermetallics, formula AXM_3, are related to both classical intermetallics of the $AuCu_3$ type and classical oxide perovskites such as $CaTiO_3$. The interstitial X elements, typically B, C, or N, can be considered either as entering the body centered position of the $AuCu_3$ cell, or as being in the transition metal (e.g. Ti in $CaTiO_3$) position in the perovskite cell. The structural and electronic analogies between $MgCNi_3$ and $CaTiO_3$ are more extensive than might be initially perceived [1]. While the T_c of $MgCNi_3$ is low ($T_c = 8$ K) compared to those of related superconductors, including $LuNi_2B_2C$ ($T_c = 16$ K) [2] and YPd_2B_2C ($T_c = 23$ K) [3], some evidence suggests that $MgCNi_3$ may represent a new type of unconventional superconductor [4], and many fundamental questions about the nature of its superconducting state remain unanswered. Of particular interest is the possible competition between magnetic and superconducting electronic ground states. As a result, there is great interest in intermetallic perovskites that are closely related to $MgCNi_3$, both in the search for new superconductors and in the pursuit of a better understanding of the interplay between superconductivity and magnetism in $MgCNi_3$.

To date, little is known about the electronic and magnetic properties of perovskite borides and carbides that are closely related to $MgCNi_3$—those that combine non-magnetic electropositive elements (especially alkaline

*Corresponding author. Department of Chemistry, Texas A&M University, P.O. Box 30012, College Station, TX 77842-3012, USA. Fax: +979-845-4719.
E-mail address: schaak@mail.chem.tamu.edu (R.E. Schaak).

0022-4596/$ - see front matter © 2003 Elsevier Inc. All rights reserved.
doi:10.1016/j.jssc.2003.10.032

earth metals) with late transition metals. Likewise, no previous studies have exhaustively addressed the synthesis of these materials, which is a necessary prerequisite to studying their properties. In this report, we explore the formation of intermetallic perovskite borides and carbides AXM_3 (A = Mg, Ca, Sc, Y, Lu, Zr, Nb; X = B, C; M = Ni, Ru, Rh, Pd, Pt) and report several new compounds. Further, we show that many of these new compounds exist over a wide range of stoichiometries, which could critically influence their superconducting properties. Finally, we present a preliminary report of the existence of superconductivity in samples with the composition CaB_xPd_3 ($x \geqslant 1$) and NbB_xRh_3, which may be attributed to unidentified impurity phases.

2. Experimental

2.1. Synthesis

All AXM_3 compounds (A = Mg, Ca, Sc, Y, Lu, Zr, Nb; X = B, C; M = Ni, Ru, Rh, Pd, Pt) were synthesized either by arc melting or by standard powder techniques. For arc melted samples, starting materials were bright Mg flakes, freshly cleaved metal lumps (Ca, Sc, Y, Lu), metal foil (Zr, Nb), buttons of pre-melted metal powders (Ni, Ru, Rh, Pd, Pt), lump boron, and ca. 2 mm graphite pieces. For neutron diffraction studies, lumps of isotope-enriched ^{11}B were used. For powder syntheses, starting materials were bright Mg flakes, freshly cleaved Ca lumps, −325 mesh metal powders (Ni, Ru, Rh, Pd, Pt), amorphous submicron boron powder, and glassy carbon spherical powder. All elements were at least 99.9% pure. Alkaline earth and rare earth metals were stored under argon, and exposure to air during handling was minimized.

The formation of all AXM_3 compounds was first attempted by arc melting 0.25 g samples under Ar on a water-cooled copper hearth. The melted buttons were turned over and melted a total of three times to ensure homogeneity. The samples were analyzed both as-melted and after annealing at 1100°C in evacuated silica tubes for 2–5 days. For A = Mg, the high volatility of Mg made arc melting difficult, so these samples were also prepared by placing the powders in dense alumina crucibles and heating to 900°C in an evacuated silica tube for several days. Both arc melting and powder syntheses were attempted for A = Ca. For A = Mg and Ca, a 15% excess of the alkaline earth metal was used for both the arc melting and powder syntheses to compensate for loss due to volatilization.

2.2. Characterization

All samples were initially analyzed by room-temperature powder X-ray diffraction using Cu$K\alpha$ radiation. Selected samples in the systems CaB_xPd_3, $LuCPd_3$ and MgB_xPd_3 were analyzed by neutron powder diffraction. Neutron powder diffraction data were collected on the Special Environment Powder Diffractometer at the Intense Pulsed Neutron Source at Argonne National Laboratory. Samples were finely ground before data collection to avoid the influence of preferred orientation and contained in thin-walled vanadium cans. The average data collection time was 16 h per sample. High-resolution backscattering data ($2\theta = 144.85°$, Bank 1) were analyzed using the Rietveld refinement method with the GSAS (EXPGUI) suite.

Electron microscopy was performed on $NbBRh_3$ samples. Electron transparent areas were obtained by crushing, suspending in ethanol, and placing a few droplets on a Cu grid with a holey C film. Electron diffraction studies were performed with a Philips CM300UT-FEG and a Philips CM200ST-FEG electron microscope, both with a field emission gun. Nanodiffraction was performed using a condenser aperture of 10 μm and an electron probe size of 4–10 nm in diameter. Imaging and elemental analysis was performed on FEI Dual Beam 235, equipped with an EDAX elemental analysis system.

The resistivities of polycrystalline samples in the Ca–Pd–B system were measured down to temperatures of 0.3 K by standard four-point resistivity measurements. The specific heats in the vicinity of the 1 K superconducting transition in CaB_xPd_3 were measured by the semiadiabatic heat pulse method in a custom-made apparatus, and by the same method in a commercial apparatus for $NbBRh_3$.

3. Results and discussion

3.1. Formation of intermetallic perovskites

We explored the formation of intermetallic boride and carbide perovskites AXM_3 (A = Mg, Ca, Sc, Y, Lu, Zr, Nb; X = B, C; M = Ni, Ru, Rh, Pd, Pt) under the two sets of conditions that we found to be the most robust. The compositions were chosen to combine electropositive elements with non-magnetic late transition metal elements to yield structural and electronic analogues to $MgCNi_3$. Powder techniques were used for A = Mg and Ca, and all other samples were prepared by arc melting. (Attempts were made to prepare A = Ca samples by both arc melting and powder syntheses. Unless otherwise specified, all results for A = Ca are reported for the arc melted samples.) Figs. 1 and 2 summarize our findings for borides and carbides, respectively, showing the compositions that form a perovskite phase along with those that do not under our synthetic conditions. In these figures, distinctions are made between samples that appear to be single phase by X-ray diffraction at a

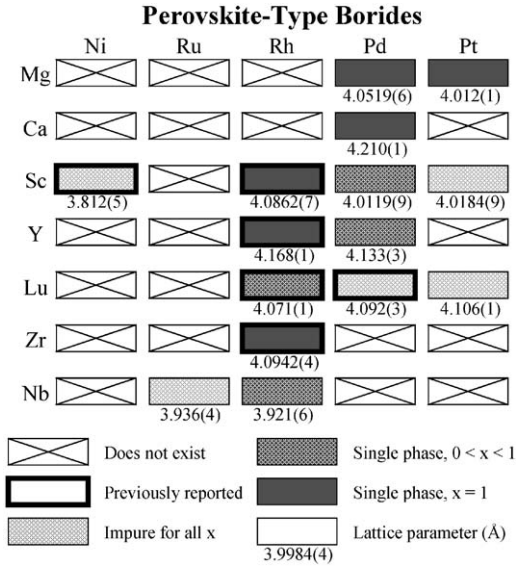

Fig. 1. Chart summarizing the formation of selected intermetallic perovskite borides using arc melting and standard powder techniques. Samples that were at least 95% pure by X-ray diffraction were considered to be single-phase.

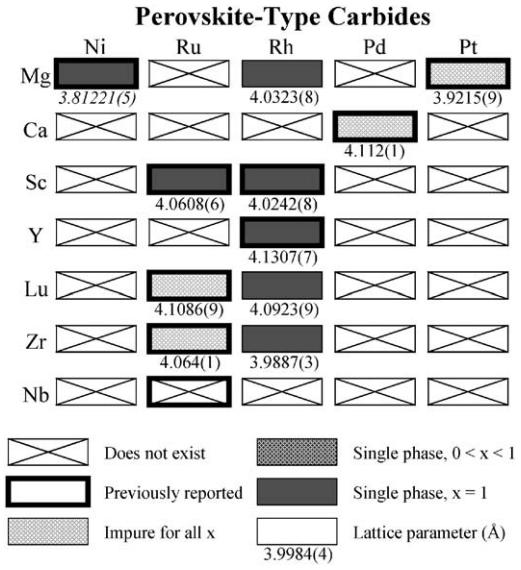

Fig. 2. Chart summarizing the formation of selected intermetallic perovskite carbides using arc melting and standard powder techniques. Samples that were at least 95% pure by X-ray diffraction were considered to be single-phase.

nominally *stoichiometric* composition (AXM_3) and those that appear to be single phase only at a *substoichiometric* nominal composition ($AX_{1-\delta}M_3$), as well as those that are multi-phase at all compositions. Lattice parameters are reported for the largest attainable unit cell for each system, which corresponds to the maximum boron or carbon content. For samples that were arc melted, the reported lattice parameters are for the as-melted samples. Unless otherwise specified, annealing produced no observable change in lattice constant or phase purity. For comparison, binary compositions that form in the related $AuCu_3$ structure type are indicated in Fig. 3, along with their reported lattice constants. (The $AuCu_3$ structure is identical to perovskite, except that the interstitial site is empty in $AuCu_3$ and filled in perovskite.)

Other than $MgCNi_3$, MgC_xPt_3 is the only other previously reported $MgXM_3$ perovskite (X = B, C; M = Ni, Ru, Rh, Pd, Pt) [5]. For MgC_xPt_3, the reported value of x is 0.17 [5], and our lattice parameter data confirm that MgC_xPt_3 ($a = 3.921$) is only slightly larger than $AuCu_3$-type $MgPt_3$ ($a = 3.918$) [6]. MgC_xRh_3, MgB_xPd_3, and MgB_xPt_3 exist as single-phase perovskites and are new compounds. Powder XRD patterns for MgC_xRh_3 and MgB_xPd_3 are shown in Fig. 4. The difference between the lattice constants of MgB_xPd_3 ($a = 4.052$) and MgB_xPt_3 ($a = 4.012$) suggests that the maximum boron content in MgB_xPd_3 is higher, since Pd and Pt are similar in size.

CaB_xPd_3 is a new compound, and the X-ray diffraction pattern for the $x = 1$ sample is shown in Fig. 4. Powder syntheses of $CaXM_3$ (X = B, C; M = Ni, Ru, Rh, Pd, Pt) in evacuated silica tubes did not result in the formation of any perovskite-type compounds. However, perovskite phases form in the Ca–Pd–C and Ca–Pd–B systems upon arc melting. Although Ca has a low boiling point, arc-melting Ca with Pd (and Pt) is successful, presumably because Ca reacts with Pd at low temperatures to form binary phases that are less volatile [6]. Perovskite phases were also observed in powder preparations of CaB_xPd_3 synthesized in sealed tantalum tubes. Arc melting Ca with Ru, Rh, or Ni was

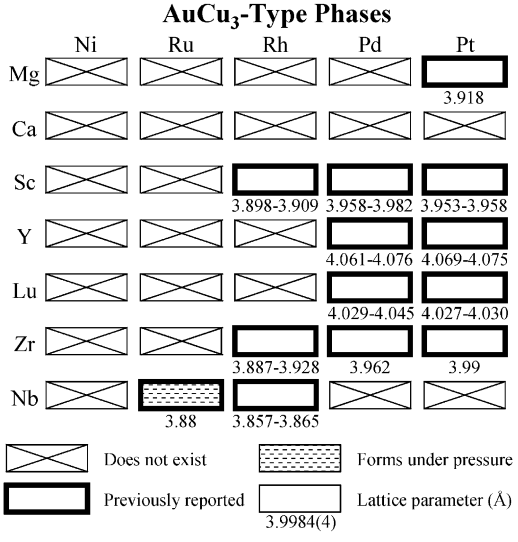

Fig. 3. Summary of previously reported $AuCu_3$-type binary phases, including reported lattice parameters (taken from Ref. [13]).

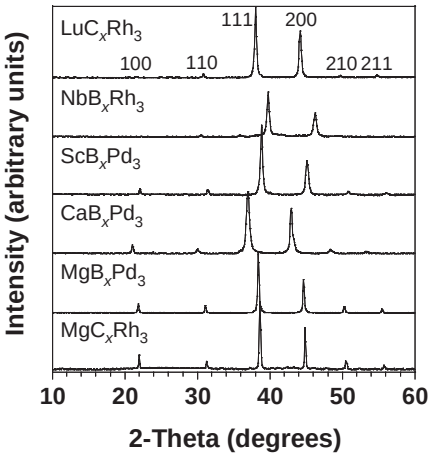

Fig. 4. Powder X-ray diffraction patterns of MgC_xRh_3, MgB_xPd_3, CaB_xPd_3, ScB_xPd_3, NbB_xRh_3, and LuC_xRh_3. For ScB_xPd_3, x is nominally 0.5. For all other compounds, $x = 1$.

much less successful and resulted in no perovskite phases. CaC_xPd_3 has been previously reported [7], although we observe a $CaPd_2$ impurity for all values of x. Likewise, the lattice constant for CaC_xPd_3 ($a = 4.112$, this work; $a = 4.141$, [7]) remains nearly constant over a wide range of nominal carbon content, suggesting that x is small.

The previously reported compounds AB_xRh_3 (A = Sc, Y, Lu, Zr) [8], along with ScB_xNi_3 [9] and LuB_xPd_3 [10], were confirmed. Under our synthetic conditions, ScB_xNi_3 and LuB_xPd_3 were impure for all x, while LuB_xRh_3 was single phase only for $x<1$. ScB_xPd_3 (Fig. 4), YB_xPd_3, and NbB_xRh_3 (Fig. 4) represent new substoichiometric perovskite phases. Attempts to prepare these as stoichiometric compounds resulted in multi-phase samples with no observed increase in lattice constants beyond the maximum single-phase value. ScB_xPt_3, LuB_xPt_3, and NbB_xRu_3 were found to exist, but only in the presence of other impurity phases.

For the carbides, the existence of single-phase ScC_xRu_3 [11], ScC_xRh_3 [12] and YC_xRh_3 [12] was confirmed. LuC_xRh_3 (Fig. 4) and ZrC_xRh_3 represent new single-phase perovskite compounds. LuC_xPd_3 is single-phase, but neutron diffraction data indicated that no carbon was incorporated into $AuCu_3$-type $LuPd_3$, so LuC_xPd_3 does not exist. We found evidence for the formation of LuC_xRu_3 and ZrC_xRu_3, but not NbC_xRu_3. The original report of the $ACRu_3$ compounds obtained single-phase materials using rapid-quenching methods [11], which were not available during this work. This suggests that other elusive compounds, or higher-purity samples, may be attainable by finding alternate or optimized synthetic procedures.

In the ternary systems under study, binary $AuCu_3$-type compounds often exist [13], and in these cases lattice parameter data provide evidence for perovskite formation. For example, both ScB_xRh_3 ($a = 4.086$) and ScC_xRh_3 ($a = 4.024$) are larger than $AuCu_3$-type $ScRh_3$ ($a = 3.909$), suggesting that boron and carbon are incorporated into the structure, forming a perovskite. Likewise, YB_xPd_3 ($a = 4.133$) is larger than YPd_3 ($a = 4.07$). However, since the unit cell of YC_xPd_3 ($a = 4.075$) is nearly the same size as that of YPd_3, we conclude that YC_xPd_3 does not form the perovskite structure. Rather, the nominal composition YC_xPd_3 forms $AuCu_3$-type YPd_3 along with unreacted carbon.

Analysis of the compositions that form a perovskite phase suggest the existence of an electronic stability region. For example, all of the carbides that form perovskites are either isoelectronic to $MgCNi_3$ (e.g. $MgCPt_3$ and $CaCPd_3$) or electron deficient (e.g. $MgCRh_3$, $ScCRu_3$, $ScCRh_3$, etc.). Likewise, the borides that form perovskites are also either isoelectronic (e.g. $ScBPd_3$) or electron deficient (e.g. $CaBPd_3$, $ScBRh_3$, $NbBRu_3$, etc.) relative to $MgCNi_3$. No perovskite that was observed in this study had more electrons per formula unit than $MgCNi_3$.

3.2. Substoichiometry of intermetallic perovskites

It is well known that intermetallic perovskite borides and carbides can exist over a wide homogeneity range. For example, ScB_xRh_3 exists as a single-phase solid solution for $0 \leqslant x \leqslant 1$ [12]. Superconducting MgC_xNi_3 is only single-phase in the range $0.88 \leqslant x \leqslant 1$ [14,15]. From a superconductivity perspective, the fact that T_c decreases linearly as x decreases from unity is crucially important [15]. In our exploration of the formation of intermetallic perovskites that are related to $MgCNi_3$, the boride and carbide contents are critical to the superconducting properties.

Fig. 5 shows a plot of lattice constant (from X-ray diffraction data) vs. nominal boron content for four new intermetallic perovskites. The unit cell of CaB_xPd_3 expands linearly with boron content for $0.25 \leqslant x \leqslant 1.0$. Above $x = 1.0$, no additional boron is incorporated into CaB_xPd_3. Likewise, the boron content of MgB_xPd_3 increases up to $x = 1$, where the lattice constant levels off. YB_xPd_3 and ScB_xPd_3 both exist as $AuCu_3$-type compounds at $x = 0$ [13], and they swell to accommodate boron up to $x = 0.5$. For $x > 0.5$, however, no additional boron uptake is observed. Thus, the X-ray diffraction data suggest that CaB_xPd_3 and MgB_xPd_3 exist as stoichiometric compounds, while YB_xPd_3 and ScB_xPd_3 are both substoichiometric.

Refinements of neutron diffraction data for the same CaB_xPd_3 samples presented in Fig. 5, however, indicate that the solubility limits are lower than revealed by X-ray diffraction. (The lattice constants of the CaB_xPd_3 samples as determined by X-ray and neutron diffraction agree to within 1.5%.) Fig. 6 shows the Rietveld refinement of the neutron diffraction data for $CaB_{1.05}Pd_3$, with the refined structure shown in the

inset. The multi-phase refinement includes predominantly CaB_xPd_3, along with a CaB_6 [0.32(2) wt%] impurity and small amounts of vanadium and cadmium from the sample can and mask used to minimize background scattering. Based on the refined neutron diffraction data, the actual boron content of the sample with a starting composition of $CaB_{1.05}Pd_3$ is actually $CaB_{0.76(1)}Pd_3$. (Some of the excess boron is unavoidably lost during the arc melting process.) Thus, CaB_xPd_3 for $x>1$ does not represent a stoichiometric compound, as suggested by the X-ray data, but rather the substoichiometric compound $CaB_{0.76(1)}Pd_3$ at the solubility limit of B in CaB_xPd_3.

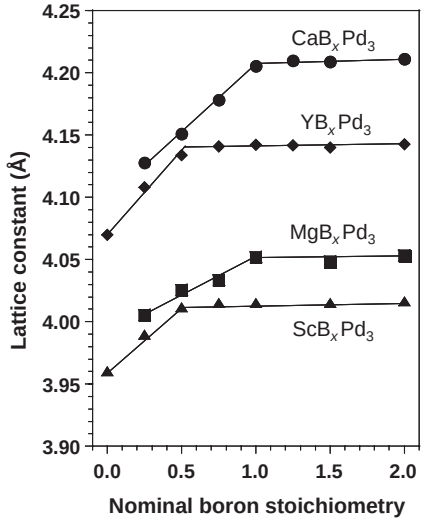

Fig. 5. Variation of the lattice constant (determined by X-ray diffraction) as a function of the nominal boron content for CaB_xPd_3, YB_xPd_3, MgB_xPd_3, and ScB_xPd_3. The error bars are all ± 0.02 or less, which is smaller than the data points on the plot.

As shown in Fig. 7, the actual boron site occupancies do not, in general, correspond with the nominal boron content, although they still confirm the linear trend in boron uptake with increasing nominal content. The maximum boron content is only $x = 0.76$, even at a nominal stoichiometric composition. Thus, even though attempts to prepare the entire solid solution CaB_xPd_3 ($0.25 \leqslant x \leqslant 1$) appeared successful by lattice parameter data obtained from X-ray diffraction measurements, neutron diffraction data confirms that stoichiometric $CaBPd_3$ is not attainable under our synthetic conditions. Preliminary attempts to increase the boron content by annealing and high pressure were unsuccessful.

Similar neutron diffraction refinements of MgB_xPd_3 revealed a boron site occupancy of $x = 0.71(1)$ for a nominal composition of $x = 1.3$. The site occupancies of YB_xPd_3 and ScB_xPd_3 were not refined since they are

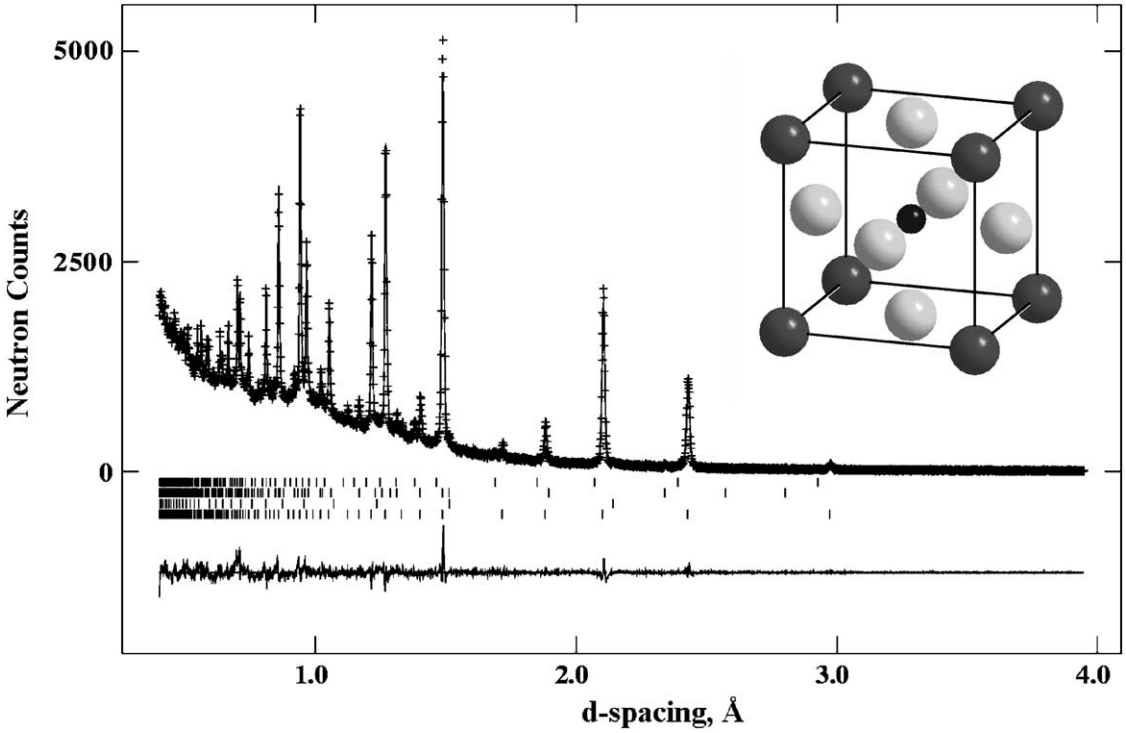

Fig. 6. Time-of-flight neutron diffraction pattern of CaB_xPd_3 for a nominal composition of $x = 1.05$ showing the observed (crosses) and calculated (solid line) intensities. The difference between the observed and calculated intensities is shown below the diffraction pattern. The tick marks (from bottom to top) indicate allowed reflections for CaB_xPd_3 (refined $x = 0.76$), vanadium, cadmium, and CaB_6. The crystal structure of CaB_xPd_3 is shown in the inset (small dark circle represents B, larger dark circles represent Ca, and light circles represent Pd). $R_p = 4.66\%$, $R_{wp} = 6.76\%$, $\chi^2 = 1.782$, $U_{iso}(Pd) = 0.0139(4)$, $U_{11}(Pd) = 0.0105(7)$, $U_{22}(Pd) = U_{33}(Pd) = 0.0146(4)$, $U_{iso}(B^{11}) = 0.0222(6)$.

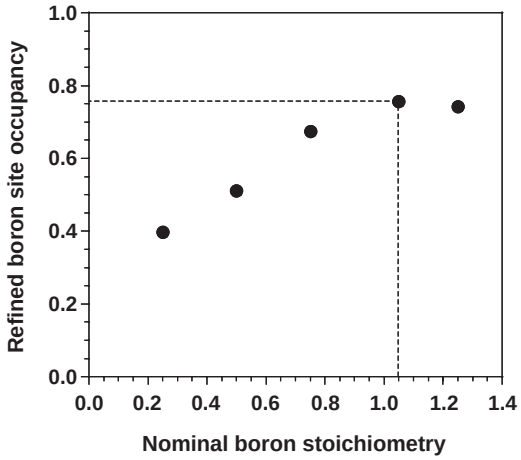

Fig. 7. Plot of the refined boron site occupancy (determined by neutron diffraction) vs. the nominal boron content for CaB_xPd_3. The error bars are all ± 0.01 or less, which is smaller than the data points on the plot.

clearly substoichiometric, based on X-ray measurements (Fig. 5). Overall, the site occupancies and composition limits may reflect either an electronic limit or a structural limitation to unit cell expansion based on the sizes and bonding preferences of the constituent elements.

3.3. Possibility of superconductivity in CaB_xPd_3 and NbB_xRh_3

All samples were tested for superconductivity down to 2 K, and some (CaB_xPd_3, MgB_xPd_3, YB_xPd_3, and ScB_xPd_3) were tested down to 0.3 K. Of these, only CaB_xPd_3 and NbB_xRh_3 showed signs of superconductivity that were not initially attributable to known superconductors.

The temperature-dependent resistivity for CaB_xPd_3 ($x = 0.75$, 1.05, 1.25) below 1.6 K is shown in Fig. 8. $CaB_{0.75}Pd_3$ is not superconducting, but $CaB_{1.05}Pd_3$ and $CaB_{1.25}Pd_3$ are superconducting with onset temperatures of 0.8 and 1.0 K, respectively. The X-ray diffraction patterns for CaB_xPd_3 ($x = 0.75$, 1.05, 1.25), shown in the inset of Fig. 8, indicate that $CaB_{0.75}Pd_3$ and $CaB_{1.05}Pd_3$ are nearly single-phase materials, although neutron diffraction does identify a small amount (0.32 wt%) of CaB_6 in the $x = 1.05$ sample. (While there are no extra peaks in the X-ray diffraction pattern for $CaB_{1.05}Pd_3$, impurity phases below the detection limit could still be present.) $CaB_{1.25}Pd_3$ clearly contains multiple phases, and the impurities remain unidentified.

Data from specific heat measurements on a bulk sample of $CaB_{1.05}Pd_3$ are shown in Fig. 9. The plot of $[C(T)/T]$ vs. T^2, shown in the inset to Fig. 9, shows no evidence for superconducting transitions above 2 K, as expected. From this plot, we estimate that $\gamma \approx 5$ mJ per mol K^{-2} for $CaB_{1.05}Pd_3$, or 1.7 mJ per mol Pd K^{-2}. This

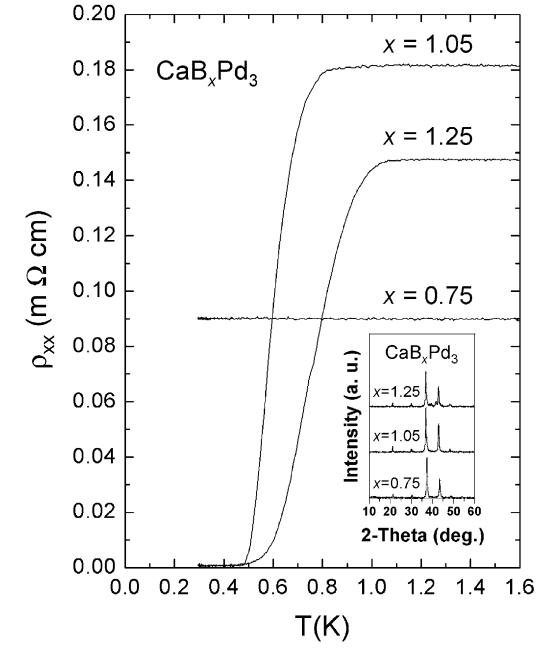

Fig. 8. Temperature-dependent resistivity for CaB_xPd_3 ($x = 0.75, 1.05, 1.25$) below 1.6 K. Powder X-ray diffraction patterns of CaB_xPd_3 ($x = 0.75, 1.05, 1.25$) are shown in the inset.

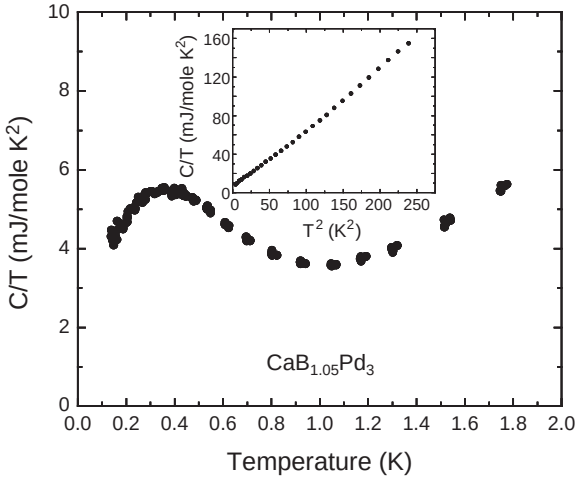

Fig. 9. Characterization of the superconducting transition of $CaB_{1.05}Pd_3$ by specific heat. A plot of $C(T)/T$ vs. T below 2 K is shown in the main panel, and a plot of $C(T)/T$ vs. T^2 is shown in the inset.

value for γ is much lower than that for $MgCNi_3$ ($\gamma \approx 10$ mJ per mol Ni K^{-2}). The plot of $[C(T)/T]$ vs. T below 2 K for $CaB_{1.05}Pd_3$ is shown in Fig. 9. While there is a broad feature centered at 0.4 K, the signal is very weak, and the broad hump in Fig. 9 could also be attributed to spin fluctuations. Along those lines, the peak in C/T vs. T at 0.4 K shifts to higher temperatures in an applied field, which argues that the peak is due to spin fluctuations rather than superconductivity. Thus,

there is no clear evidence of a bulk superconducting transition in $CaB_{1.05}Pd_3$. Therefore, the superconducting phase is likely to be present in small quantities in the sample, possibly as an intergranular phase that runs throughout the bulk sample.

In an attempt to identify and isolate the superconducting phase in CaB_xPd_3, samples that spanned a variety of compositions within the Ca–B–Pd ternary system were synthesized. The samples were chosen to account for the possibility of boron doping into common Ca-Pd binary phases ($CaPd_2B_{0.2}$, $Ca_3Pd_2B_{0.2}$, and $CaPdB_{0.2}$) or microscopic doping into CaB_6 ($CaB_{5.94}C_{0.06}$ and $CaB_{5.95}Pd_{0.05}$, prepared by powder techniques at 900°C). Samples of Ca_2Pd_3B, $CaPd_4B$, $CaPd_3B_2$, $CaPd_{12}B_6$, and $CaPd_{0.5}B_5$ were made to explore different regions of Ca–Pd–B phase space. No samples showed signs of superconductivity down to 0.3 K.

These results suggest that the superconductor is most likely a Ca–Pd–B ternary phase, since attempts to produce superconductors based on Ca–Pd, Pd–B, and Ca–B binary phases were unsuccessful. Given that γ for $CaB_{1.05}Pd_3$ is much smaller than for $MgCNi_3$, a T_c near 1 K would not be unexpected for perovskite-type CaB_xPd_3. Since the maximum boron content of CaB_xPd_3 ($x = 0.76$) is below the minimum value of x required for superconductivity to occur in MgC_xNi_3 [1,15], there is a realistic possibility that regions of an inhomogeneous CaB_xPd_3 sample have a sufficient boron content to be superconducting. More synthetic work and characterization are required to explore this possibility.

Superconductivity was also observed in samples of NbB_xRh_3. The plot of DC magnetization vs. temperature in Fig. 10 shows a sharp transition to a diamagnetic state below 6.4 K. The superconducting phase fraction appears to be very large. However, as in the case of CaB_xPd_3, the specific heat data (Fig. 10) indicate either that only a small percentage of the NbB_xRh_3 phase is superconducting, or that the superconductivity must be attributed to an impurity phase. Microstructure analysis by electron microscopy, shown in Fig. 11, shows two distinct phases—a bulk phase with the composition NbB_xRh_3 ($x = 0.2$) surrounded by thin sections of another phase with the composition $NbRh_2B_{2-y}$ ($0 \leqslant y \leqslant 0.3$). Thus, it is impossible at this point to determine whether NbB_xRh_3 or $NbRh_2B_{2-y}$ is the superconducting phase in this sample. More detailed analysis is in progress.

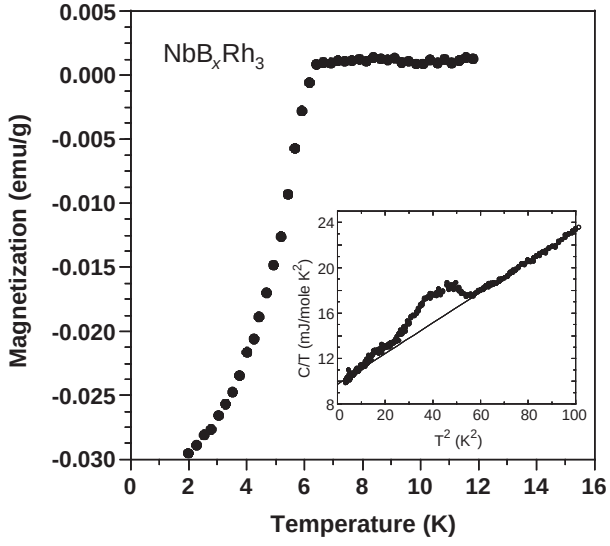

Fig. 10. Plot of DC magnetization vs. temperature for NbB_xRh_3. Inset: specific heat measurement of NbB_xRh_3 showing $C(T)/T$ vs. T^2.

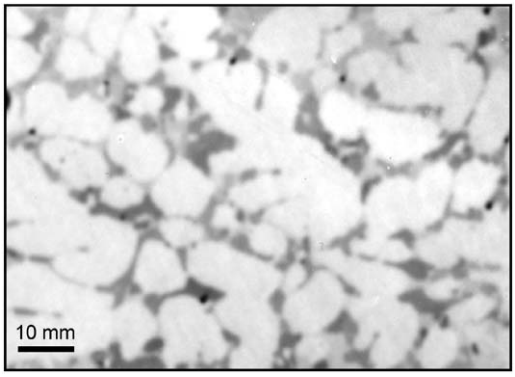

Fig. 11. TEM image of NbB_xRh_3. The white areas have the composition $NbB_{0.2}Rh_3$. The gray phase at the grain boundaries is $NbRh_2B_{2-y}$ ($0 \leqslant y \leqslant 0.3$). The black areas are voids.

4. Conclusions

A general study of the formation of intermetallic boride and carbide perovskites related to $MgCNi_3$ was reported, and several new compounds were identified. Lattice parameter data based on X-ray diffraction studies indicate that many of these perovskites have a variable composition. Although compounds such as CaB_xPd_3 appear single-phase and boron-rich at a stoichiometric nominal composition, neutron diffraction studies indicate that saturation occurs at a substoichiometric composition. This result is critical to the realization of superconductivity in intermetallic perovskites, since the superconducting T_c of MgC_xNi_3 decreases rapidly with decreasing carbon content. Preliminary evidence suggests that a superconductor ($T_c < 1$ K) exists in the Ca–Pd–B ternary system, and while this may be attributed to perovskite-type CaB_xPd_3, synthetic improvements and more careful characterization are required to substantiate this claim. Further, samples with the composition NbB_xRh_3 also showed superconductivity, but the superconducting signal could be either from NbB_xRh_3 or $NbRh_2B_{2-y}$.

Acknowledgments

The work at Princeton University was supported by the US Department of Energy, grant DE-FG02-98ER45706, along with funds from NSF-MRSEC grant DMR 0213706. The work at Argonne National Laboratory was supported by the US Department of Energy, Office of Basic Energy Sciences—Materials Sciences, under contract No. W-31-109-ENG-38. Work at Los Alamos was supported by a Laboratory-Directed Research and Development grant. HWZ acknowledges financial support by Stichting voor Fundamenteel Onderzoek der Materie (FOM).

References

[1] T. He, Q. Huang, A.P. Ramirez, Y. Wang, K.A. Regan, N. Rogado, M.A. Hayward, M.K. Haas, J.S. Slusky, K. Inumara, H.W. Zandbergen, N.P. Ong, R.J. Cava, Nature 411 (2001) 54.

[2] R.J. Cava, H. Takagi, H.W. Zandbergen, J.J. Krajewski, W.F. Peck, T. Siegrist, B. Batlogg, R.B. Vandover, R.J. Felder, K. Mizuhashi, J.O. Lee, H. Eisaki, S. Uchida, Nature 367 (1994) 252; R. Nagarajan, C. Mazumdar, Z. Hossain, S.K. Dhar, K.V. Gopalakhrishnan, L.C. Gupta, C. Godart, B.D. Padalia, R. Vijayaraghavan, Phys. Rev. Lett. 72 (1994) 274.

[3] R.J. Cava, H. Takagi, B. Batlogg, H.W. Zandbergen, J.J. Krajewski, W.F. Peck, R.B. Vandover, R.J. Felder, T. Siegrist, K. Mizuhashi, J.O. Lee, H. Eisaki, S.A. Carter, S. Uchida, Nature 367 (1994) 146.

[4] M. Sigrist, K. Voelker, cond-mat/0208367, 2002.

[5] H.H. Stadelmaier, W.K. Hardy, Z. Metallkd. 52 (1961) 391.

[6] T.B. Massalski (Ed.), Binary Alloy Phase Diagrams, Vol. 3, ASM International, Materials Park, OH, 1996.

[7] U.E. Musanke, W. Jeitschko, Z. Naturforsch. B 46 (1991) 1177.

[8] H. Holleck, J. Less-Common Met. 52 (1977) 167;
H. Takei, N. Kobayashi, H. Yamauchi, T. Shishido, T. Fukase, J. Less-Common Met. 125 (1986) 233;
H. Takei, T. Shishido, J. Less-Common Met. 97 (1984) 223;
P. Rogl, H. Nowotny, J. Less-Common Met. 67 (1979) 41.

[9] I.R. Shein, A.L. Ivanovskii, N.I. Medvedeva, JETP Lett. 74 (2001) 122; Yu.B. Kuz'ma, Crystal Chemistry of Borides, Vishcha Shkola, Lvov, 1983.

[10] S.K. Dhar, S.K. Malik, R. Vijayaraghavan, Mater. Res. Bull. 16 (1981) 1557.

[11] H. Holleck, Metall (Berlin) 37 (1983) 475.

[12] T. Shishido, J. Ye, K. Kudou, S. Okada, K. Obara, T. Sugawara, M. Oku, K. Wagatsuma, H. Horiuchi, T. Fukuda, J. Alloys Compd. 291 (1999) 52.

[13] P. Villars, L.D. Calvert (Eds.), Pearson's Handbook of Crystallographic Data for Intermetallic Phases, 2nd Edition, ASM International, Materials Park, OH 1991.

[14] E. Scheil, L. Huetter, Z. Metallkd. 44 (1953) 387;
L.J. Hueter, H.H. Stadelmaier, Acta Metall. 6 (1958) 367.

[15] T.G. Amos, Q. Huang, J.W. Lynn, T. He, R.J. Cava, Solid State Commun. 121 (2002) 73.